Original Article

Journal of LOW FREQUENCY NOISE, VIBRATION AND ACTIVE CONTROL

Journal of Low Frequency Noise, Vibration and Active Control
0(0) 1–15

DOI: 10.1177/1461348419867524
journals.sagepub.com/home/lfn
SAGE

An improved neuroendocrine–proportional–integral–derivative controller with sigmoid-based secretion rate for nonlinear multi-input–multi-output crane systems

Mohd Riduwan Ghazali[1], Mohd Ashraf Ahmad[1], Raja Mohd Taufika Raja Ismail[1] and M Osman Tokhi[2]

Abstract

This paper proposes an improved neuroendocrine–proportional–integral–derivative controller for nonlinear multi-input–multi-output crane systems using a sigmoid-based secretion rate of the hormone regulation. The main advantage of the sigmoid-based secretion rate neuroendocrine–proportional–integral–derivative is that the hormone secretion rate of neuroendocrine–proportional–integral–derivative can be varied according to the change of error. As a result, it can provide high accuracy control performance, especially in nonlinear multi-input–multi-output crane systems. In particular, the hormone secretion rate is designed to adapt with the changes of error using a sigmoid function, thus contributing to enhanced control accuracy. The parameters of the sigmoid-based secretion rate neuroendocrine–proportional–integral–derivative controller are tuned using the safe experimentation dynamics algorithm. The performance of the proposed sigmoid-based secretion rate neuroendocrine–proportional–integral–derivative controller-based safe experimentation dynamics algorithm is evaluated by tracking the error and the control input. In addition, the performances of proportional–integral–derivative and neuroendocrine–proportional–integral–derivative controllers are compared with the proposed sigmoid-based secretion rate neuroendocrine–proportional–integral–derivative performance. From the simulation work, it is discovered that the sigmoid-based secretion rate neuroendocrine–proportional–integral–derivative design provides better control performances in terms of the objective function, the total norm of error and the total norm of input compared to proportional–integral–derivative and neuroendocrine–proportional–integral–derivative controllers. In particular, it is shown the proposed sigmoid-based secretion rate neuroendocrine–proportional–integral–derivative controller contributes 5.12% of control accuracy improvement by changing the fixed hormone secretion rate into a variable hormone secretion rate based on the change of error.

Keywords

Sigmoid, neuroendocrine, secretion rate, data driven, nonlinear system

Introduction

Nowadays, nonlinear multi-input–multi-output (MIMO) crane systems are widely used in the container logistics industry for loading and unloading containers from and to container ships in the harbour. During the loading and unloading process, the crane requires a highly accurate controller to control the payload oscillations and payload

[1]Instrumentation and Control Engineering Research Cluster (ICE), Faculty of Electrical and Electronics Engineering (FKEE), Universiti Malaysia Pahang (UMP)Pekan, Pahang, Malaysia
[2]School of Engineering, London South Bank University, London UK

Corresponding author:
Mohd Riduwan Ghazali, Instrumentation and Control Engineering Research Cluster (ICE), Faculty of Electrical and Electronics Engineering (FKEE), Universiti Malaysia Pahang (UMP), 26600 Pekan, Pahang, Malaysia.
Email: riduwan@ump.edu.my

bouncing to avoid any cause of damage or accidents. Various controller methods have been proposed to achieve accurate movement. These include sliding mode control,[1] linear quadratic regulator (LQR) control,[2] feedback control,[3] H-infinity control,[4] proportional–integral–derivative (PID) with input shaping,[5] and fuzzy-sliding mode control.[6] Generally, most of the controller designs are model based, where the control is derived from mathematical model of the system, and this is very challenging and complicated in case of nonlinear dynamic systems.[7] Thus, model-based control methods potentially suffer from problems of un-modelled dynamics, which lead to model inaccuracy and hence poor control performance.

A data-driven control scheme is a suitable alternative option since it does not depend on the model of the system in designing the controller.[8,9] A data-driven control scheme is designed using the input and output data only and treats the system as a black box. Meanwhile, the data-driven control based on PID control is commonly chosen due to its simple structure, ease of implementation and fewer number of parameters to tune, and that it allows to be used for a wide range of operating conditions.[10,11] However, the PID controller has some limitations in controlling a complex nonlinear system, especially at nonlinear MIMO crane system. This is due to the fact that the PID structure is linear in nature and it is unable to adapt with the complex nonlinear system.[12] Thus, large numbers of published studies have proposed advanced PID controllers, such as fractional PID,[13] neural network PID,[14] fuzzy PID,[15] sigmoid PID[16,17] and fractional order sliding mode PID.[18]

On the other hand, the controllers that were inspired by nature in biological phenomena have also been proposed to improve the conventional PID. This include brain emotional learning (BEL),[19] neuro-dynamics control,[20] immune system control[21] and neuroendocrine control.[22,23] From the aforementioned, the neuroendocrine–PID (NEPID) control has shown great potential in providing high control accuracy and performance in controlling nonlinear MIMO systems.[24] Based on our preliminary study,[25] the NEPID also shows a promising results for nonlinear MIMO gantry crane system. Generally, the NEPID control is a combination of neuroendocrine with the PID control that is likely to result in more efficient and better control performance as compared to the standard PID control. The neuroendocrine is derived from general secretion rules of the hormone in the human body that has the form of a hill function.[22,26] This hormone regulation mechanism can be generalized and modified mathematically, which can then be applied to control systems by embedding an additional bio-inspired section to the existing PID controller. However, in the existing version of the NEPID, the parameter of hormone secretion rate is constant during the whole simulation or experiment time. Hence, it is worth to improve the existing NEPID by varying the hormone secretion rate parameter according to the change in control variable error. In particular, it is proposed in this study to modify the fixed hormone secretion rate to variable secretion rate according to the changes of the control variable error by using a sigmoid function. Therefore, designing the variable hormone secretion rate of neuroendocrine–PID control could offer a great potential in improving the control accuracy of the standard NEPID controller in controlling nonlinear MIMO crane systems.

This paper presents a sigmoid-based secretion rate neuroendocrine–PID (SbSR–NEPID) control mechanism for controlling nonlinear MIMO crane systems. The parameters of SbSR–NEPID are tuned using safe experimentation dynamics (SED) in the data-driven control framework. The SED optimization method is a game theoretic method that randomly perturbs several elements of the design parameter to search for the optimal design parameter.[27] The essential feature of the SED method is that it is able to provide stable convergence and better control accuracy by keeping the best parameter value in the updating process. Moreover, the coefficients of the SED method are independent of the number of iterations and thus robust to disturbances or delays during the tuning process. Therefore, the SED method has good capability to find the optimal SbSR–NEPID parameters and thus produce a better control performance. The performance of the proposed control approach is validated through application to a nonlinear MIMO crane system in terms of tracking error and control input energy. Underpinning this novel technique, the contribution of this work is to verify that the SbSR–NEPID provides better control performance accuracy than the standard NEPID and the standard PID controller by modifying the fixed secretion rate into variable secretion rate based on a sigmoid function. Hence, the new version of NEPID could offer more effective neuroendocrine regulation that can track the changes of control error.

The rest of the organization of this research paper is organised presented as follows. The second section presents the given nonlinear MIMO crane system and the problem formulation of the data-driven SbSR–NEPID controller. In the third section, SbSR–NEPID control design based on SED-based method is explained. The proposed controller is then validated with a container gantry crane system in the fourth section. The analysis and the performance comparison between the proposed controller and the standard NEPID and the standard PID controllers are also presented and discussed. Finally, the conclusions drawn from the work are presented in the fifth section.

Notation: The real number sets and the positive real number sets are denoted by $\mathbb{R}$ and $\mathbb{R}_+$, respectively. The symbol $\mathbb{R}^n$ represents the set of n real numbers. $\mathbf{0}$ and $\mathbf{1}$ are defined as vector whose all elements are zero and one, respectively.

Problem formulation

In this section, the nonlinear MIMO crane system is firstly described. Then, the problem setting of the proposed SbSR–NEPID controller for the MIMO crane system is presented.

Container gantry crane system

Figure 1 shows a container gantry crane system for swing motion of the payload caused by trolley movement[28,29] in which X represents the direction of motion of the trolley and Z is the vertical direction. The outputs $x(t)$, $l(t)$, and $\theta(t)$ are the trolley displacement, rope length and sway angle of the payload, respectively. Then, $F_x(t)$ and $F_l(t)$ refer to the control inputs of trolley force in X-direction and hoist force in l-direction, respectively. The equations of motion of the crane are given as follows:

$$\dot{\boldsymbol{x}}_a = f(\boldsymbol{x}_a) + g(\boldsymbol{x}_a)\boldsymbol{u}_a \tag{1}$$

and

$$\boldsymbol{y} = C\boldsymbol{x}_a \tag{2}$$

where

$$\boldsymbol{x}_a = \begin{bmatrix} x & l & \theta & \dot{x} & \dot{l} & \dot{\theta} \end{bmatrix}^{\mathrm{T}} \tag{3}$$

The function $f(\boldsymbol{x}_a)$ is given as

$$f(\boldsymbol{x}_a) = \begin{bmatrix} \boldsymbol{q}_2 \\ -M^{-1}(\boldsymbol{q})[V_m(\boldsymbol{q}, \dot{\boldsymbol{q}})\dot{\boldsymbol{q}} + G(\dot{\boldsymbol{q}})] \end{bmatrix} \tag{4}$$

where $\boldsymbol{q}_1 = \boldsymbol{q}$, $\boldsymbol{q}_2 = \dot{\boldsymbol{q}}$, $\boldsymbol{u} = [F_x \quad F_l \quad 0]^{\mathrm{T}}$ and $\boldsymbol{q} = [x \quad l \quad \theta]^{\mathrm{T}}$. The function $g(\boldsymbol{x}_a)$ is

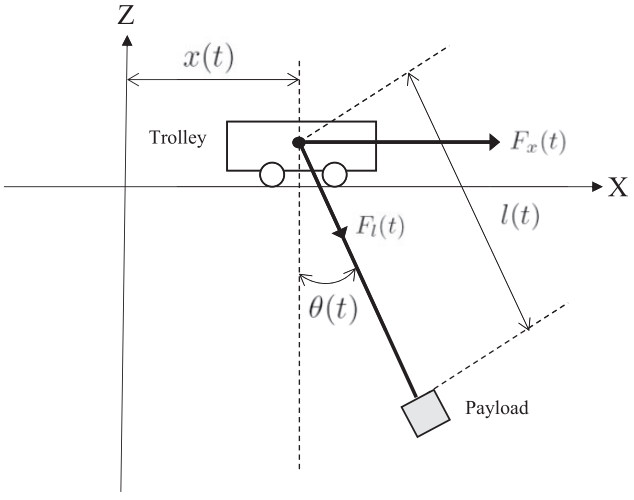

Figure 1. The container gantry crane system.

$$g(\boldsymbol{x}_a) = -h(\boldsymbol{x}_a)E_0 \tag{5}$$

where $h(\boldsymbol{x}_a) = \begin{bmatrix} 0_{3\times3} \\ -M^{-1}(\boldsymbol{q}) \end{bmatrix}$, $E_0 = \begin{bmatrix} 1 & 0 & 0 \\ 0 & 1 & 0 \end{bmatrix}^{\mathrm{T}}$ and $\boldsymbol{u}_a(t) = [u_1 \quad u_2]^{\mathrm{T}} = [F_x \quad F_l]^{\mathrm{T}}$. The general equation of container gantry crane is given as

$$M(\boldsymbol{q})\ddot{\boldsymbol{q}} + V_m(\boldsymbol{q}, \dot{\boldsymbol{q}})\dot{\boldsymbol{q}} + G(\dot{\boldsymbol{q}}) = \boldsymbol{u} \tag{6}$$

where

$$M(\boldsymbol{q}) = \begin{bmatrix} m_p + m_t & m_p \sin\theta & m_p l\cos\theta \\ m_p \sin\theta & m_p + m_l & 0 \\ m_p l\cos\theta & 0 & m_p l^2 + I \end{bmatrix} \tag{7}$$

$$V_m(\boldsymbol{q}, \boldsymbol{q}.) = \begin{bmatrix} 0 & m_p\dot{\theta}\cos\theta & -m_p l\sin\theta\dot{\theta} + m_p\cos\theta\dot{l} \\ 0 & 0 & -m_p l\dot{\theta} \\ 0 & m_p l\dot{\theta} & m_p l\dot{l} \end{bmatrix} \tag{8}$$

and

$$G(\dot{\boldsymbol{q}}) = \begin{bmatrix} 0 & -m_p g\cos\theta & m_p g l\sin\theta \end{bmatrix}^{\mathrm{T}} \tag{9}$$

Then, the output of container gantry crane is

$$\boldsymbol{y} = \begin{bmatrix} 1 & 0 & 0 & 0 & 0 & 0 \\ 0 & 1 & 0 & 0 & 0 & 0 \\ 0 & 0 & 1 & 0 & 0 & 0 \end{bmatrix} \begin{bmatrix} x \\ l \\ \theta \\ \dot{x} \\ \dot{l} \\ \dot{\theta} \end{bmatrix} = \begin{bmatrix} x \\ l \\ \theta \end{bmatrix} = \boldsymbol{q} \tag{10}$$

The parameters of the system considered are $m_p = 0.73$ kg, $m_t = 1.06$ kg, $m_l = 0.5$ kg and $I = 0.005$ kgm^2. Note that, this model has been verified using actual gantry crane system as reported in Park et al.[28]

Problem setting

Consider the SbSR–NEPID control for MIMO crane system as shown in Figure 2, where $\boldsymbol{r}(t) \in \mathbb{R}^b$ is a reference, $\boldsymbol{u}(t) \in \mathbb{R}^a$ is control input, $\boldsymbol{d}(t) \in \mathbb{R}^b$ is deterministic disturbance, $\boldsymbol{y}(t) \in \mathbb{R}^b$ is output measurement and $\boldsymbol{e}(t) \in \mathbb{R}^b$ is error between reference and system output. The MIMO crane system is denoted by symbol H, where a and b represent the number of inputs and outputs of the system, respectively. t_s is sampling time for

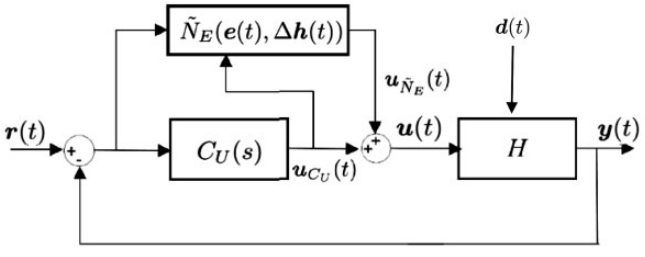

Figure 2. The SbSR–NEPID control system.

$t = 0, t_s, 2t_s, 3t_s \ldots Dt_s$, where D is the number of samples. The SbSR–NEPID is a combination of standard PID controller unit $C_U(s)$ and sigmoid-based secretion rate of neuroendocrine $\tilde{N}_E(\boldsymbol{e}(t), \Delta\boldsymbol{h}(t))$ controller. The controller $C_U(s)$ for the MIMO crane system is defined as

$$C_U(s) = \begin{bmatrix} C_{11}(s) & \ldots & C_{1b}(s) \\ \vdots & \ddots & \vdots \\ C_{a1}(s) & \ldots & C_{ab}(s) \end{bmatrix} \tag{11}$$

where

$$C_{ij}(s) = K_{Pij}\left(1 + \frac{1}{K_{Iij}s} + \frac{K_{Dij}s}{\left(K_{Dij}/N_{ij}\right)s}\right) \tag{12}$$

is the PID controller for $i = 1, 2 \ldots a$ and $j = 1, 2 \ldots b$. The PID parameters $K_{Pij} \in \mathbb{R}$, $K_{Iij} \in \mathbb{R}$, $K_{Dij} \in \mathbb{R}$ and $N_{ij} \in \mathbb{R}$ are the proportional gain, integral time, derivative time and filter coefficient, respectively. The output of $C_U(s)$ is denoted as

$$\boldsymbol{u}_{C_U}(t) = \left[\sum_{j=1}^{b} h_{1j}, \quad \sum_{j=1}^{b} h_{2j}, \quad \ldots \quad \sum_{j=1}^{b} h_{aj}\right]^{\mathrm{T}} \tag{13}$$

where $h_{ij} = C_{ij}(s)e_j(t)$ and $e_j(t) = r_j(t) - y_j(t)$.

The $\tilde{N}_E(\boldsymbol{e}(t), \Delta\boldsymbol{h}(t))$ is given as

$$\tilde{N}_E(\boldsymbol{e}(t), \Delta\boldsymbol{h}(t)) = \begin{bmatrix} \tilde{V}_{11}(e_1(t), \Delta h_{11}(t)) & \ldots & \tilde{V}_{1b}(e_b(t), \Delta h_{b1}(t)) \\ \vdots & \ddots & \vdots \\ \tilde{V}_{a1}(e_1(t), \Delta h_{a1}(t)) & \ldots & \tilde{V}_{ab}(e_b(t), \Delta h_{ab}(t)) \end{bmatrix} \tag{14}$$

where

$$\tilde{V}_{ij}\left(e_j(t), \Delta h_{ij}(t)\right) = \tilde{\alpha}_{ij}\left[\frac{\left(|\Delta h_{ij}(t)|\right)^{\zeta_{ij}}}{\lambda_{ij} + \left(\left(|\Delta h_{ij}(t)|\right)^{\zeta_{ij}}\right)} + \beta_{ij}\right] L_1 L_2 \tag{15}$$

and

$$L_1 = -\frac{e_j(t)}{|e_j(t)|}\frac{\Delta e_j(t)}{|\Delta e_j(t)|}, \quad L_2 = \frac{\Delta h_{ij}(t)}{|\Delta h_{ij}(t)|} \tag{16}$$

such that $\Delta h_{ij}(t) = h_{ij}(t) - h_{ij}(t - t_s)$ is the variance of $h_{ij}(t)$ and the change of error is $\Delta e_j(t) = e_j(t) - e_j(t - t_s)$. The symbol ζ_{ij} is a hill coefficient while β_{ij} and λ_{ij} are scalar positive real numbers. Note that, $\tilde{V}_{ij}\left(e_j(t), \Delta h_{ij}(t)\right) = 0$ would be fulfilled if $\Delta h_{ij}(t) = 0$, so all $\beta_{ij} = 0$.[22] The direction factors L_1 and L_2 of equation (16) are used to abolish the error effectively by ensuring the output of the controller is always against the changing direction of the error where the value is either 1 or -1. The hormone secretion intensity of equation (15) is monotonous and non-negative, which has the form of a hill function as given by Ding et al.[22] The variable coefficient of secretion rate $\tilde{\alpha}_{ij}$ is based on sigmoid function given by

$$\tilde{\alpha}_{ij} = \alpha_{ij\min} + \frac{\left|\alpha_{ij\max} - \alpha_{ij\min}\right|}{1 + \mathrm{e}^{-\gamma_{ij}\left(e_j(t) - \epsilon_{ij}\right)}} \tag{17}$$

where $\alpha_{ij\min} \in \mathbb{R}$ and $\alpha_{ij\max} \in \mathbb{R}$ are the lower and the upper bounds of $\tilde{\alpha}_{ij}$, respectively. The symbols γ_{ij} and ϵ_{ij} are the coefficients to adjust the sharpness of curve and to shift the centre of curve between lower and upper bounds, respectively. For simplicity of design parameter tuning, $\Delta\alpha_{ij} = \left|\alpha_{ij\max} - \alpha_{ij\min}\right|$. Then, the output of $\tilde{N}_E(\boldsymbol{e}(t), \Delta\boldsymbol{h}(t))$ is denoted by

$$\underset{\sim}{\boldsymbol{u}}_{\tilde{N}_E}(t) = \left[\sum_{j=1}^{b} \widetilde{V}_{1j}, \quad \sum_{j=1}^{b} \widetilde{V}_{2j}, \quad \ldots \quad \sum_{j=1}^{b} \widetilde{V}_{aj}\right]^{\mathrm{T}} \tag{18}$$

Thus, the combination of the signals $\boldsymbol{u}_{\boldsymbol{C}_U}(t)$ and $\boldsymbol{u}_{\tilde{N}_E}(t)$ produce the output of SbSR–NEPID controller as

$$\boldsymbol{u}(t) = \boldsymbol{u}_{C_U}(t) + \boldsymbol{u}_{\tilde{N}_E}(t) \tag{19}$$

where $\boldsymbol{u}(t) = [u_1(t), u_2(t), \ldots, u_a(t)]^{\mathrm{T}}$, $\boldsymbol{u}_{C_U}(t) \in \mathbb{R}^a$ and $\boldsymbol{u}_{\tilde{N}_E}(t) \in \mathbb{R}^a$.

Remarks 2.1: Note that, the value of $\tilde{\alpha}_{ij}$ in equation (17) is varied according to the signal $e_j(t)$, instead of using fix coefficient in the standard NEPID.[22,25,26] Moreover, a unique value of curve sharpness and shifting curve (γ and ϵ) are considered for each $\tilde{\alpha}$ which do not give any restriction to error signal $\boldsymbol{e}(t)$ in equation (17). Therefore, the sigmoid based secretion rate has more flexibility to provide a better control accuracy of SbSR–NEPID as compared to the standard NEPID.

Next, the system in Figure 2 is observed for its performance index based on

$$\bar{e_j} := \int_{t_0}^{t_f} \left|(r_j(t) - y_j(t)\right|^2 \mathrm{d}t \tag{20}$$

$$\bar{u}_i := \int_{t_0}^{t_f} |u_i(t)|^2 \mathrm{d}t \tag{21}$$

where $r_j(t)$, $y_j(t)$ and $u_i(t)$ are the elements j and i for vectors $\boldsymbol{r}(t)$, $\boldsymbol{y}(t)$ and $\boldsymbol{u}(t)$, respectively. The time interval $[t_0, t_f]$ is referred as the duration for the evaluation of performance where $t_0 \in \{0\} \cup \mathbb{R}_+$ and $t_f \in \mathbb{R}_+$. The definition of the objective function is given as follows

$$J(\boldsymbol{K_P}, \boldsymbol{K_I}, \boldsymbol{K_D}, \boldsymbol{N}, \zeta, \lambda, \alpha_{\min}, \Delta\alpha, \gamma, \epsilon) = \sum_{j=1}^{b} w_{1j}\bar{e}_j + \sum_{i=1}^{a} w_{2i}\bar{u}_i \tag{22}$$

where the value of the parameters $\boldsymbol{K_P} := [K_{P11}, K_{P12} \ldots, K_{pad}]^T$, $\boldsymbol{K_I} := [K_{I11}, K_{I12}, \ldots, K_{Iab}]^{\mathrm{T}}$, $\boldsymbol{K_D} := [K_{D11}, K_{D12}, \ldots, K_{Dab}]^{\mathrm{T}}$, $\boldsymbol{N} := [N_{11}, N_{12}, \ldots, N_{ab}]^{\mathrm{T}}$, $\zeta := [\zeta_{11}, \zeta_{12}, \ldots, \zeta_{ab}]^{\mathrm{T}}$, $\lambda := [\lambda_{11}, \lambda_{12}, \ldots, \lambda_{ab}]^{\mathrm{T}}$, $\alpha_{\min} := [\alpha_{11\min}, \alpha_{12\min}, \ldots, \alpha_{ab\min}]^{\mathrm{T}}$, $\Delta\alpha := [\Delta\alpha_{11}, \Delta\alpha_{12}, \ldots, \Delta\alpha_{ab}]^{\mathrm{T}}$, $\gamma := [\gamma_{11}, \gamma_{12}, \ldots, \gamma_{ab}]^{\mathrm{T}}$ and $\epsilon := [\epsilon_{11}, \epsilon_{12}, \ldots, \epsilon_{ab}]^{\mathrm{T}}$. The weighting output and input coefficients are $w_{1j} \in \mathbb{R} \quad (j = 1, 2, \ldots, b)$ and $w_{2i} \in \mathbb{R} \quad (i = 1, 2, \ldots, a)$ respectively. The symbols a and b represent the dimension of input $\boldsymbol{u}(t)$ and output $\boldsymbol{y}(t)$, respectively. The tracking error and the input energy control for control performance are consistent with the right side of equation (22).

Problem 2.1. For the control system in Figure 2, find a SbSR–NEPID controller $C_U(s)$ and $\tilde{N}_E(\boldsymbol{e}(t), \Delta\boldsymbol{h}(t))$ of nonlinear MIMO crane system, which minimizes $J(\boldsymbol{K_P}, \boldsymbol{K_I}, \boldsymbol{K_D}, \boldsymbol{N}, \zeta, \lambda, \alpha_{\min}, \Delta\alpha, \gamma, \epsilon)$ with respect to $\boldsymbol{K_P}, \boldsymbol{K_I}, \boldsymbol{K_D}, \boldsymbol{N}, \zeta$, λ, $\alpha_{\min}$, $\Delta\alpha$, γ and ϵ according to the data obtained from the measurement of $\boldsymbol{u}(t)$ and $\boldsymbol{y}(t)$.

Design of SbSR–NEPID using SED algorithm

In this section, the detailed solution of Problem 2.1 is presented. Firstly, the SED algorithm, which is used to tune the control parameters of SbSR–NEPID is presented. Secondly, the execution of the data-driven SbSR–NEPID control design method for minimizing the control objective in equation (22) is described.

Safe experimentation dynamics

Consider

$$\min_{\boldsymbol{p}\in\mathbb{R}^n} f(\boldsymbol{p}) \tag{23}$$

as an optimization problem that minimizes the objective function f by tuning the design parameter $\boldsymbol{p} \in \mathbb{R}^n$. Then, the optimal solution is obtained using the SED algorithm by continually updating the design parameter. The updated law of the SED algorithm is

$$p_i(k+1) = \begin{cases} h(\bar{p}_i - K_g rv_2), & \text{if } rv_1 \leq E, \\ \bar{p}_i, & \text{if } rv_1 > E \end{cases} \tag{24}$$

where $k = 1, 2, \ldots, k_{\max}$ is the iteration number, $p_i \in \mathbb{R}$ represents the ith element of $\boldsymbol{p} \in \mathbb{R}^n$, $\bar{p}_i \in \mathbb{R}$ represents the ith element of $\bar{\boldsymbol{p}} \in \mathbb{R}^n$ and $\bar{\boldsymbol{p}}$ is for storing the present best value of the design parameters. The symbol $k_{\max}$ is the maximum number of iterations set by the designer. The symbol K_g represents a scalar that defines the interval size to make decision on the random steps in $p_i \in \mathbb{R}$ and E is a scalar that defines the probability of using a new random setting for $\boldsymbol{p}$. Note that, $rv_1 \in \mathbb{R}$ is the random number that has been uniformly selected between 0 and 1, while $rv_2 \in \mathbb{R}$ is the new random number which has been uniformly selected between $p_{\min}$ and $p_{\max}$. The function $h(\bar{p}_i - K_g rv_2)$ in equation (24) is defined as follows

$$h(\bullet) = \begin{cases} p_{\max}, & \text{if } \bar{p}_i - K_g rv_2 < p_{\max}, \\ \bar{p}_i - K_g rv_2, & \text{if } p_{\min} \leq \bar{p}_i - K_g rv_2 \leq p_{\max}, \\ p_{\min}, & \text{if } \bar{p}_i - K_g rv_2 < p_{\min} \end{cases} \tag{25}$$

The steps of the SED method are as follows:

Step 1: Determine the values of $p_{\max}$, $p_{\min}$, K_g and E. Then, set $k = 0$ and the initial condition for the design parameter as $\boldsymbol{p}(0)$ and the corresponding objective function be $f(\boldsymbol{p}(0))$. Next, execute $\bar{\boldsymbol{p}} = \boldsymbol{p}(0)$ and $\bar{f} = f(\boldsymbol{p}(0))$. The variable $\bar{f}$ is denoted as the current best value of the objective function.
Step 2: If $f(\boldsymbol{p}(k)) \leq \bar{f}$, execute $\bar{\boldsymbol{p}} = \boldsymbol{p}(k)$ and $\bar{f} = f(\boldsymbol{p}(k))$. If not, proceed to **Step 3**.
Step 3: Generate a random number rv_1 and execute the updated law in equation (24).
Step 4: Obtain the objective function $f(\boldsymbol{p}(k+1))$.
Step 5: If the pre-stated termination condition is satisfied, the optimal design parameter

$$\boldsymbol{p}_{\text{opt}} := \arg \min_{\boldsymbol{p}\in\{\boldsymbol{p}(0),\boldsymbol{p}(1),\ldots,\boldsymbol{p}(k+1)\}} f(\boldsymbol{p}) \tag{26}$$

is recorded. If not, set $k = k + 1$ and go to **Step 2**.

The pre-stated termination condition is based on the maximum number of iterations $k_{\max}$.

Note that, in equation (25), the symbols $p_{\max}$ and $p_{\min}$ are the upper bound and the lower bound of the design parameter values. The allowable boundaries of search space $p_{\max}$ and $p_{\min}$ are determined after several preliminary experiments of the optimization problem. The guidelines to select the values of K_g and E are given in Marden et al..[30] In particular, for any probability $E < 1$, if the exploration rate K_g is sufficiently small, then $\boldsymbol{p}_{\text{opt}}$ in equation (26) can be obtained with sufficiently large number of iterations k. Therefore, a large value of $k_{\max}$ is chosen to guarantee that the $\boldsymbol{p}_{\text{opt}}$ is obtained. Here, the value of $k_{\max}$ can be determined whenever the convergence curve is almost saturated.

Data-driven sigmoid-based secretion rate neuroendocrine–PID design

In order to accelerate the exploration of the design parameter searching, a logarithmic scale is employed for the design parameter $\boldsymbol{p}$. So, the SbSR–NEPID control parameters are stated as

$$\psi = [\boldsymbol{K_P}, \boldsymbol{K_I}, \boldsymbol{K_D}, \boldsymbol{N}, \zeta, \lambda, \alpha_{\min}, \Delta\alpha, \gamma, \epsilon] \in \mathbb{R}^n \tag{27}$$

where each element of ψ is given by $\psi_i = 10^{p_i} (i = 1, 2, \ldots, n)$. Then, the objective function is written as $f = [10^{p_1}\ 10^{p_2}\ \ldots\ 10^{p_n}]^{\mathrm{T}}$. Finally, the procedure for data-driven SbSR–NEPID is given as follows:

Step 1: Let $f(\boldsymbol{p}) = J(\boldsymbol{K_P}, \boldsymbol{K_I}, \boldsymbol{K_D}, \boldsymbol{N}, \zeta, \lambda, \alpha_{\min}, \Delta\alpha, \gamma, \epsilon)$ and $p_i = \log\psi_i$. Then, the maximum iteration number $k_{\max}$ is determined.
Step 2: Implement the SED algorithm for the objective function in equation (22).
Step 3: After $k_{\max}$ is reached, the optimal output $\boldsymbol{p}_{\text{opt}} = \bar{\boldsymbol{p}}(k_{\max})$ is obtained. Then, $\psi_{\text{opt}} = [10^{p_{1\text{opt}}}\ 10^{p_{2\text{opt}}}\ \ldots\ 10^{p_{n\text{opt}}}]^{\text{T}}$ is applied to $C_U(s)$ and $\tilde{N}_E(\boldsymbol{e}(t), \Delta\boldsymbol{h}(t))$ in the SbSR–NEPID control system in Figure 2.

Numerical example

In this section, the performance investigation of the data-driven SbSR–NEPID controller based on the SED method for nonlinear container crane system is presented. The performance of the SbSR–NEPID is compared with the standard NEPID and the standard PID controllers. Each performance controller is evaluated based on the following criteria:

1. The analysis of the objective function $J(\boldsymbol{K_P}, \boldsymbol{K_I}, \boldsymbol{K_D}, \boldsymbol{N}, \zeta, \lambda, \alpha_{\min}, \Delta\alpha, \gamma, \epsilon)$, the total norm of error $\sum_{j=1}^{3} \bar{e}_j$ and the total norm of input $\sum_{i=1}^{2} \bar{u}_i$.
2. The control performance accuracy comparison between the SbSR–NEPID and the NEPID controller. Specifically, the percentage of the control accuracy improvement J_Λ is calculated as

$$\%J_\Lambda = \frac{|J_{SbSR-NEPID} - J_{NEPID}|}{J_{NEPID}} \times 100\% \tag{28}$$

Next, the container gantry crane system in Figure 1 is considered, where the number of inputs $a = 2$ and the number of outputs $b = 3$. The input and output of the crane system are defined by $u_1(t) = F_x(t)$, $u_2(t) = F_l(t)$, $y_1(t) = x(t)$, $y_2(t) = l(t)$ and $y_3(t) = \theta(t)$, respectively. In order to validate the effectiveness of proposed SbSR–NEPID controller, the desired position is set as

$$\boldsymbol{r}(t) = [0 \quad 0.2 \quad 0]^{\text{T}} \forall t \tag{29}$$

Here, the SbSR–NEPID controller $C_U(s)$ and $\tilde{N}_E(\boldsymbol{e}(t), \Delta\boldsymbol{h}(t))$ are considered as follows:

$$C_U(s) = \begin{bmatrix} C_{11}(s) & 0 & C_{13}(s) \\ 0 & C_{22}(s) & 0 \end{bmatrix} \tag{30}$$

and

$$\tilde{N}_E(\boldsymbol{e}(t), \Delta\boldsymbol{h}(t)) = \begin{bmatrix} \tilde{V}_{11} & 0 & \tilde{V}_{13} \\ 0 & \tilde{V}_{22} & 0 \end{bmatrix} \tag{31}$$

The dimension of the SbSR–NEPID controller parameters for equations (30) and (31) is $n = 30$. The corresponding design parameter $\psi := [\boldsymbol{K_P}, \boldsymbol{K_I}, \boldsymbol{K_D}, \boldsymbol{N}, \zeta, \lambda, \alpha_{\min}, \Delta\alpha, \gamma, \epsilon] \in \mathbb{R}^{30}$ is tabulated in Table 1. The aim here is to find the $\psi \in \mathbb{R}^{30}$ that minimizes the performance index J in equation (22) for $w_{11} = 200, w_{12} = 400, w_{13} = 200$, $w_{21} = 1$ and $w_{22} = 1$. The time for the final simulation is set as $t_f = 20$ s and the total number of iterations is $k_{\max} = 3000$. The coefficients of the SED are $K_g = 0.022$, $E = 0.66$, $p_{\min} = -4$ and $p_{\max} = 4$. The initial $\boldsymbol{p}(0)$ is selected based on several preliminary experiments and the values are given in Table 1.

Remarks 3.1: In order to fairly compare our proposed controller with the standard NEPID and PID controllers, we also adopt the SED method with similar coefficients, performance indexes, weighting coefficients and maximum number of iterations to tune both NEPID and PID controllers.

Figure 3 shows the objective function J response of the SbSR–NEPID controller based on the SED method for $k_{\max} = 3000$ iterations. It justifies that the SED-based method is capable of minimizing the objective function and produces optimal SbSR–NEPID control parameters $\boldsymbol{p}_{\text{opt}}$ as stated in Table 1. Furthermore, the output responses

Table 1. Design parameters.

ψ	SbSR–NEPID	$p(0)$	$10^{p(0)}$	p_{opt}	$10^{p_{opt}}$
ψ_1	K_{P11}	−0.08	0.832	−0.022	0.950
ψ_2	K_{I11}	1.3	19.953	1.602	40.022
ψ_3	K_{D11}	0.2	1.585	0.126	1.338
ψ_4	N_{11}	0.7	5.012	1.313	20.573
ψ_5	ζ_{11}	0.3	1.995	0.547	3.525
ψ_6	λ_{11}	−2	0.010	−2.160	0.007
ψ_7	α_{min11}	0.3	1.995	0.191	1.553
ψ_8	$\Delta\alpha_{11}$	1	10.000	0.660	4.572
ψ_9	γ_{11}	0.2	1.585	0.385	2.426
ψ_{10}	ϵ_{11}	0.3	1.995	0.342	2.197
ψ_{11}	K_{P13}	−2.4	0.004	−2.005	0.010
ψ_{12}	K_{I13}	−2.5	0.003	−2.353	0.004
ψ_{13}	K_{D13}	−1	0.100	−1.221	0.060
ψ_{14}	N_{13}	1.1	12.589	1.083	12.103
ψ_{15}	ζ_{13}	0	1.000	0.021	1.048
ψ_{16}	λ_{13}	−1.9	0.013	−1.916	0.012
ψ_{17}	α_{min13}	0.5	3.162	0.538	3.455
ψ_{18}	$\Delta\alpha_{13}$	1	10.000	0.946	8.821
ψ_{19}	γ_{13}	0.2	1.585	0.068	1.169
ψ_{20}	ϵ_{13}	0.1	1.259	0.321	2.093
ψ_{21}	K_{P22}	0.6	3.981	0.840	6.921
ψ_{22}	K_{I22}	−0.2	0.631	−0.398	0.400
ψ_{23}	K_{D22}	−0.2	0.631	−0.353	0.444
ψ_{24}	N_{22}	0.1	1.259	0.507	3.210
ψ_{25}	ζ_{22}	0.7	5.012	0.762	5.782
ψ_{26}	λ_{22}	−1.1	0.079	−1.006	0.099
ψ_{27}	α_{min22}	0	1.000	0.418	2.615
ψ_{28}	$\Delta\alpha_{22}$	1	10.000	0.815	6.534
ψ_{29}	γ_{22}	0.1	1.259	−0.017	0.961
ψ_{30}	ϵ_{22}	0	1.000	0.103	1.266

SbSR–NEPID: sigmoid-based secretion rate neuroendocrine–proportional–integral–derivative.

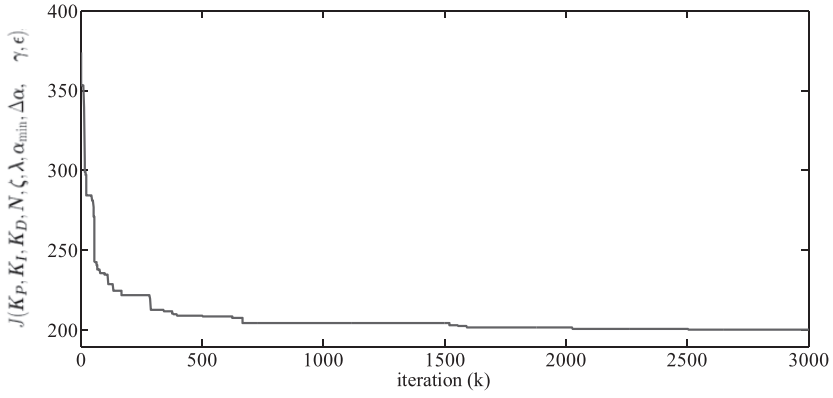

Figure 3. The objective function, *J* for container gantry crane.

of the crane system $y_1(t)$, $y_2(t)$ and $y_3(t)$ controlled by SbSR–NEPID controller are demonstrated in Figures 4, 5 and 6, respectively, while the control input responses u_1 and u_2 are shown in Figures 7 and 8, respectively. Here, all the responses are compared with the standard PID controller and the standard NEPID controller. The thin dash gray in the figures indicates the reference, the dash gray line represents the response with PID controller, the dot black line represents the response with NEPID and the solid black line indicates the response with SbSR–NEPID controller. It is clearly seen that the data-driven SbSR–NEPID is able to produce better trolley

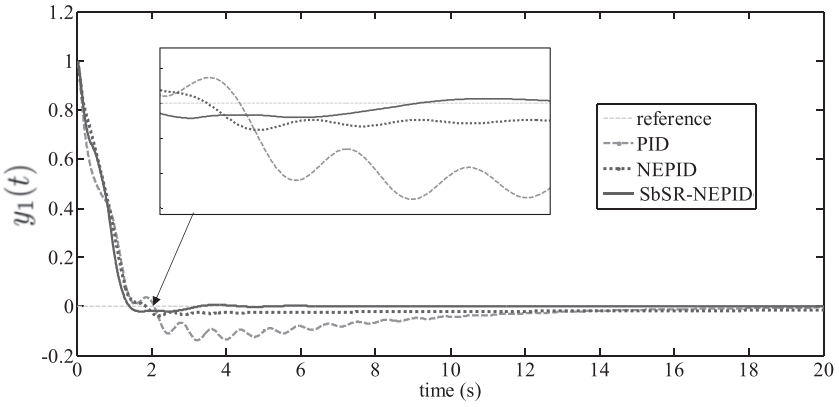

Figure 4. Trolley displacement $y_1(t)$ responses.

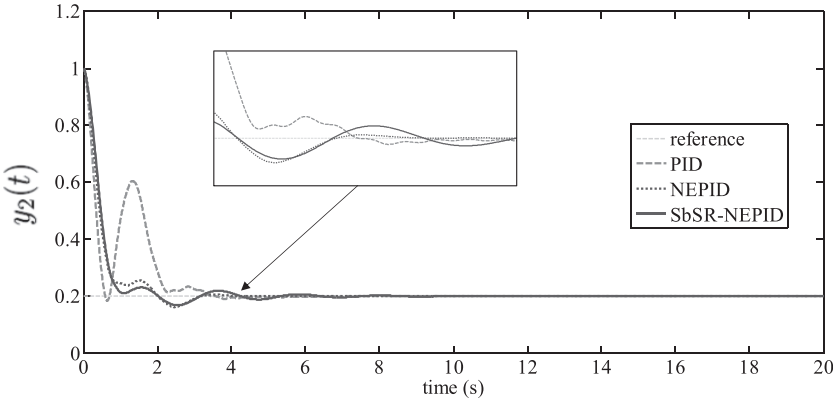

Figure 5. Rope length $y_2(t)$ responses.

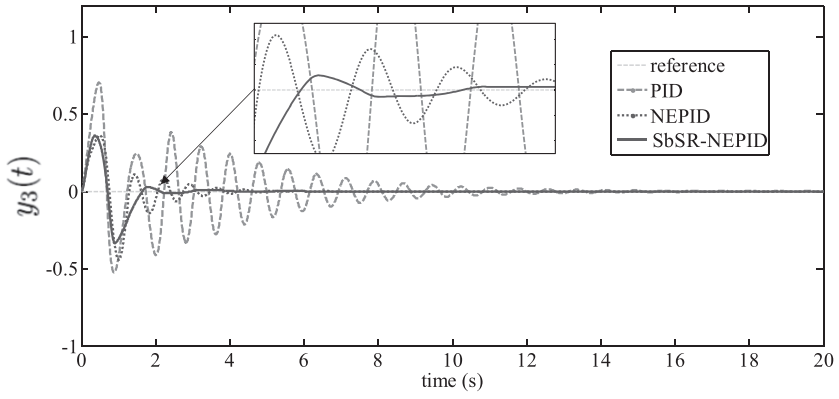

Figure 6. Sway angle of the payload $y_3(t)$ responses.

displacement $y_1(t)$ and rope length $y_2(t)$ responses based on the lower overshoot and less settling time as compared to the PID and NEPID controllers. Meanwhile, the sway angle $y_3(t)$ response shows reduced oscillations and fast settling time as compared to the NEPID and PID controller. It can further be seen that the SbSR–NEPID controller produces less control input energy $u_1(t)$ and $u_2(t)$ in order to control the MIMO crane system.

All the above findings are also supported by the numerical analysis shown in Table 2. The results show that the objective function J, the total of norm error $\sum_{j=1}^{3} \bar{e}_j$ and the total of norm input $\sum_{i=1}^{2} \bar{u}_i$ from the proposed

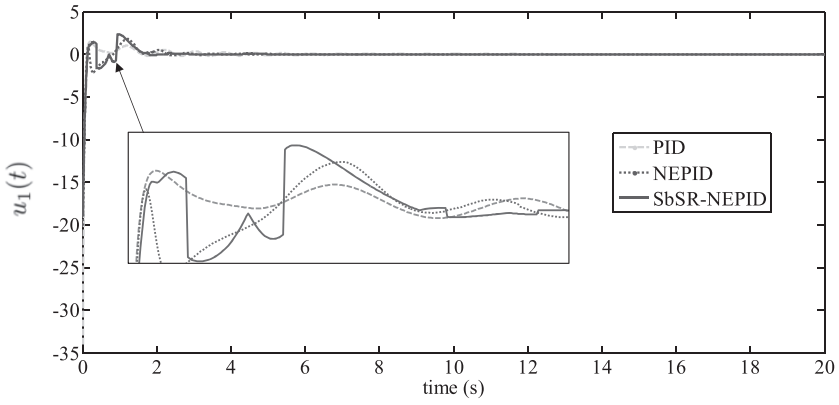

Figure 7. The trolley force, $u_1(t)$ responses.

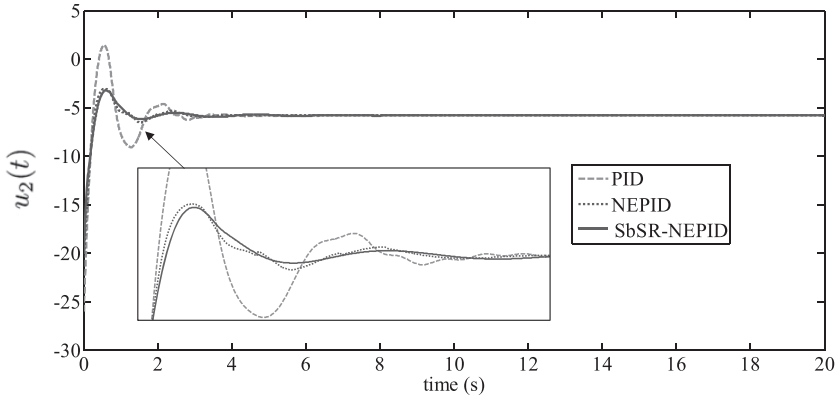

Figure 8. The hoist force, $u_2(t)$ responses.

Table 2. Numerical result of container gantry crane system.

Controller	PID	NEPID	SbSR–NEPID
J	333.1457	211.2734	*200.4576*
$\sum_{j=1}^{3} \bar{e}_j$	1.0775	0.7336	*0.6802*
$\sum_{i=1}^{2} \bar{u}_i$	70.1729	30.2694	*27.4562*

PID: proportional–integral–derivative; SbSR–NEPID: sigmoid-based secretion rate neuroendocrine–proportional–integral–derivative.

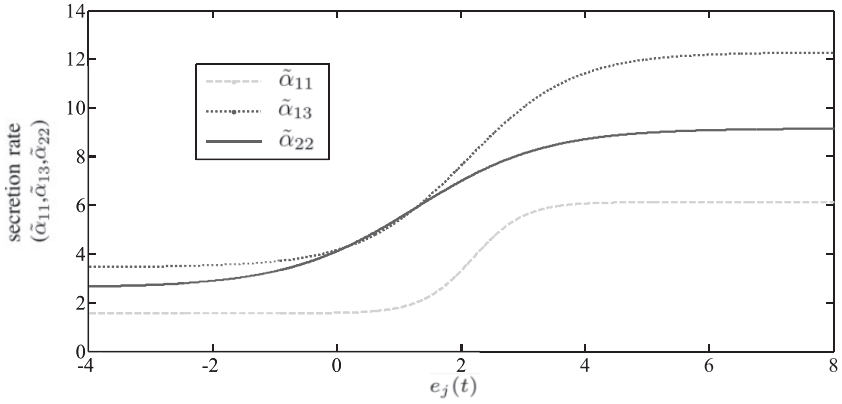

Figure 9. The sigmoid function of $\tilde{\alpha}_{11}$, $\tilde{\alpha}_{13}$ and $\tilde{\alpha}_{22}$.

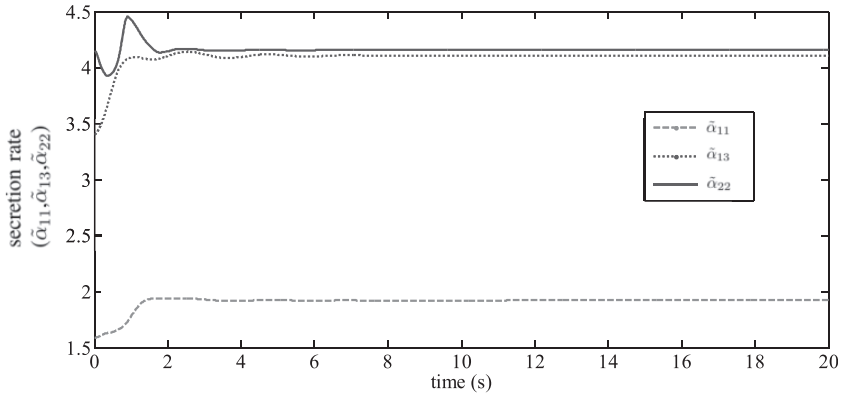

Figure 10. The hormone secretion rate responses of $\tilde{\alpha}_{11}$, $\tilde{\alpha}_{13}$ and $\tilde{\alpha}_{22}$ in SbSR–NEPID.

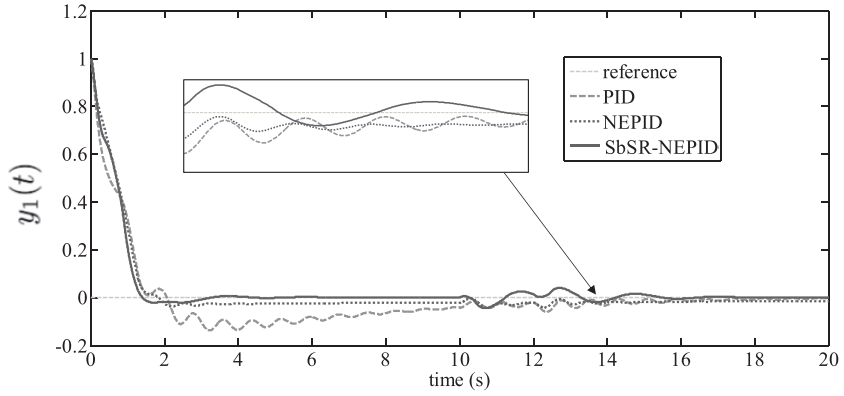

Figure 11. Trolley displacement $y_1(t)$ with disturbance.

SbSR–NEPID controller produce slightly lower values in comparison to the standard PID and standard NEPID controller. Moreover, the control accuracy improvement J_Λ of SbSR–NEPID as compared to the standard NEPID was obtained as 5.12%. This proves the significance of introducing the variable secretion rate based on sigmoid function into the NEPID controller.

The optimal hormone secretion rate functions $\tilde{\alpha}_{11}$, $\tilde{\alpha}_{13}$ and $\tilde{\alpha}_{22}$ are shown in Figure 9. It noted that lower magnitude of secretion rates $\tilde{\alpha}_{11}$, $\tilde{\alpha}_{13}$ and $\tilde{\alpha}_{22}$ are required for the range of errors between -4 and 0. The values of secretion rates start to increase in the range of error between 0 and 4, before settling at some high magnitude values for errors greater than 4. Figure 10 shows the responses of the hormone secretion rate as a function of time. This indicates that the hormone secretion rate varied during 0–2 s due to the high error that occurred in transient responses. Meanwhile, the value of hormone secretion rates settled at some optimum values after 2 s since the error already converged to zero at the steady state. These findings show the effectiveness of the new hormone secretion rate $\tilde{\alpha}_{11}$, $\tilde{\alpha}_{13}$ and $\tilde{\alpha}_{22}$ in regulating the hormone secretion intensity $\tilde{V}_{11}$, $\tilde{V}_{13}$ and $\tilde{V}_{22}$ (in equation (15)) to reduce the high magnitude of error during the transient state. Thus, this mechanism contributes to the control accuracy improvement of the controller. Thence, it is justified that the SbSR–NEPID controller is able to produce better control performance as compared to the standard NEPID and the standard PID for nonlinear MIMO crane system.

On the other hand, we also investigate the proposed SbSR–NEPID controller structure with disturbance $\boldsymbol{d}(t) = \begin{bmatrix} 0 & 0 & d_{y_3}(t) \end{bmatrix}^{\mathrm{T}}$. This disturbance is applied to the sway angle $y_3(t)$ given as follows

$$d_{y_3}(t) = \begin{cases} 0, & \text{if } 0 < t < 10, \\ 0.2, & \text{if } 10 \leq t \leq 12, \\ 0, & \text{if } 12 < t < 20 \end{cases} \tag{32}$$

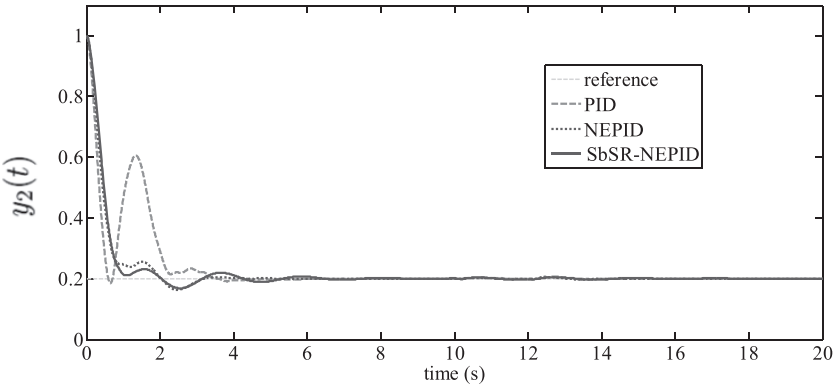

Figure 12. Rope length $y_2(t)$ with disturbance.

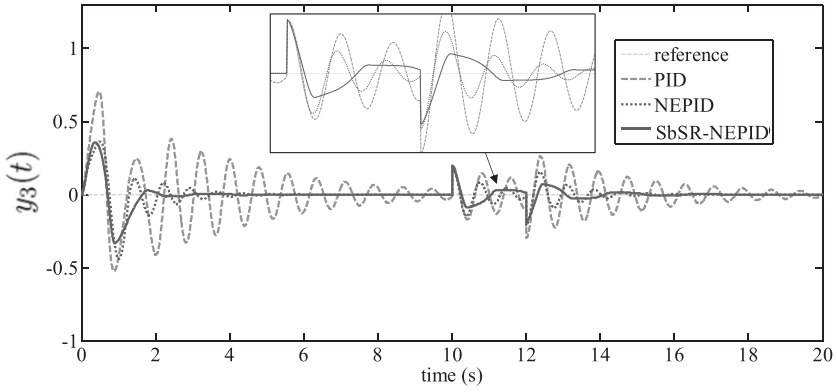

Figure 13. Sway angle $y_3(t)$ with disturbance.

Then, Figures 11, 12 and 13 show the responses of the controller in the same line configuration as in Figures 4, 5 and 6. This simulation result demonstrates that the SbSR–NEPID is able to handle disturbance at $y_3(t)$. In particular, the SbSR–NEPID provides slightly less sway angle oscillation as compared to the standard NEPID and PID controllers. At the same time, the proposed controller also able to maintain the trolley displacement and rope length according to the given desired position. Thus, it proofs that SbSR–NEPID has improved the NEPID controller in the existence of disturbance.

Conclusion

An improved NEPID controller for nonlinear MIMO crane system using a sigmoid-based secretion rate of hormone regulation tuning by SED algorithm has been presented. The research findings indicate that the sigmoid-based secretion rate of hormone regulation is effective in reducing the error during the transient state, and this contributes significantly to improved control accuracy. It has been shown that the proposed SbSR–NEPID controller outperforms the standard NEPID and the standard PID controllers in the perspective of control performance accuracy by achieving lower objective function, total norm error and total norm input even with the existence of disturbance. Moreover, it has been shown that the SbSR–NEPID controller has achieved control accuracy improvement of 5.12% as compared to standard NEPID controller.

Declaration of conflicting interests

The author(s) declared no potential conflicts of interest with respect to the research, authorship, and/or publication of this article.

Funding

The author(s) disclosed receipt of the following financial support for the research, authorship, and/or publication of this article: This research work was conducted with the support of Research Grant RDU170104 by Universiti Malaysia Pahang under Research and Innovation Department, and Ministry of Higher Education with reference no. FRGS/1/2017/ICT02/UMP/02/2.

ORCID iD

Mohd Riduwan Ghazali https://orcid.org/0000-0002-4602-2251

References

1. Lu B, Fang Y and Sun N. Sliding mode control for underactuated overhead cranes suffering from both matched and unmatched disturbances. *Mechatronics* 2017; 47: 116–125.
2. Jafari J, Ghazal M and Nazemizadeh M. A lQR optimal method to control the position of an overhead crane. *IAES Int J Robot Automat* 2014; 3: 252.
3. Tuan LA, Cuong HM, Lee SG, et al. Nonlinear feedback control of container crane mounted on elastic foundation with the flexibility of suspended cable. *J Vibrat Contr* 2016; 22: 3067–3078.
4. Rigatos G, Siano P and Abbaszadeh M. Nonlinear h-infinity control for 4-dof underactuated overhead cranes. *Trans Inst Measur Contr* 2018; 40: 2364–2377.
5. Maghsoudi M, Mohamed Z, Tokhi M, et al. Control of a gantry crane using input-shaping schemes with distributed delay. *Trans Inst Measur Contr* 2017; 39: 361–370.
6. Ngo QH, Nguyen NP, Nguyen CN, et al. Fuzzy sliding mode control of an offshore container crane. *Ocean Eng* 2017; 140: 125–134.
7. Ramli L, Mohamed Z, Abdullahi AM, et al. Control strategies for crane systems: a comprehensive review. *Mech Syst Signal Process* 2017; 95: 1–23.
8. Goodall P, Sharpe R and West A. A data-driven simulation to support remanufacturing operations. *Comput Indust* 2019; 105: 48–60.
9. Hou ZS and Wang Z. From model-based control to data-driven control: survey, classification and perspective. *Informat Sci* 2013; 235: 3–35.
10. Ahmad MA, Azuma S and Sugie T. Performance analysis of model-free PID tuning of MIMO systems based on simultaneous perturbation stochastic approximation. *Exp Syst Appl* 2014; 41: 6361–6370.
11. Yamamoto T, Takao K and Yamada T. Design of a data-driven PID controller. *IEEE Trans Contr Syst Technol* 2009; 17: 29–39.
12. Åström K and Hägglund T. The future of PID control. *Contr Eng Pract* 2001; 9: 1163–1175.
13. Shah P and Agashe S. Review of fractional PID controller. *Mechatronics* 2016; 38: 29–41.
14. Varshney T, Varshney R and Singh N. A DPSO-based NN-PID controller for MIMO systems. In: *Ambient communications and computer systems*. 2018, pp. 535–551.Singapore: Springer.
15. El-Samahy AA and Shamseldin MA. Brushless DC motor tracking control using self-tuning fuzzy PID control and model reference adaptive control. *Ain Shams Eng J* 2018; 9: 341–352.
16. Ahmad MA and Ismail RMTR. A data-driven sigmoid-based PI controller for buck-converter powered dc motor. In: *2017 IEEE symposium on computer applications and industrial electronics (ISCAIE)*. 2017, pp. 81–86. IEEE.
17. Ateş A, Alagöz BB, Yeroğlu C, et al. Sigmoid based PID controller implementation for rotor control. In: 2015 European *Control Conference (ECC)*. IEEE, 2015, pp. 458–463.
18. Azar AT and Serrano FE. Fractional order sliding mode PID controller/observer for continuous nonlinear switched systems with pso parameter tuning. In: *International conference on advanced machine learning technologies and applications*. Springer, 2018, pp. 13–22.
19. Sharma MK and Kumar A. Performance comparison of brain emotional learning-based intelligent controller (BELBIC) and PI controller for continually stirred tank heater (CSTH). In: *Computational advancement in communication circuits and systems*. Springer, 2015, pp. 293–301.
20. Zhu D, Zhao Y and Yan M. A bio-inspired neurodynamics based backstepping path-following control of an AUV with ocean current. *Int J Robot Automat* 2012; 27: 298–307.
21. Ding Y, Zhang T, Ren L, et al. Immune-inspired self-adaptive collaborative control allocation for multi-level stretching processes. *Inf Sci* 2016; 342: 81–95.
22. Ding Y, Xu N, Ren L, et al. Data-driven neuroendocrine ultrashort feedback-based cooperative control system. *IEEE Trans Contr Syst Technol* 2015; 23: 1205–1212.
23. Liu B, Ren L and Ding Y. A novel intelligent controller based on modulation of neuroendocrine system. In: *International symposium on neural networks*. Springer, 2005, pp. 119–124.
24. Ding Y, Chen L and Hao K. Human body based intelligent cooperative decoupling controllers. In: *Bio-inspired collaborative intelligent control and optimization*. Springer, 2018, pp. 25–80.

25. Ghazali MR, Ahmad MA, Jusof MFM, et al. A data-driven neuroendocrine-PID controller for underactuated systems based on safe experimentation dynamics. In: *Signal processing & its applications (CSPA), 2018 IEEE 14th international colloquium on IEEE*, 2018, pp. 61–66.
26. Liang X, Ding Y, Ren L, et al. Data-driven cooperative intelligent controller based on the endocrine regulation mechanism. *IEEE Trans Contr Syst Technol* 2014; 22: 94–101.
27. Marden JR, Ruben SD and Pao LY. A model-free approach to wind farm control using game theoretic methods. *IEEE Trans Contr Syst Technol* 2013; 21: 1207–1214.
28. Park H, Chwa D and Hong K. A feedback linearization control of container cranes: varying rope length. *Int J Contr Automat Syst* 2007; 5: 379.
29. Park MS, Chwa D and Eom M. Adaptive sliding-mode antisway control of uncertain overhead cranes with high-speed hoisting motion. *IEEE Trans Fuzzy Syst* 2014; 22: 1262–1271.
30. Marden JR, Young HP, Arslan G, et al. Payoff-based dynamics for multiplayer weakly acyclic games. *SIAM J Control Optim* 2009; 48: 373–396.